Biosensors and Bioelectronics 87 (2017) 108–115

Contents lists available at ScienceDirect

Biosensors and Bioelectronics

journal homepage: www.elsevier.com/locate/bios

3D origami electrochemical device for sensitive Pb^{2+} testing based on DNA functionalized iron-porphyrinic metal-organic framework

Xiu Wang [a], Chunlei Yang [a], Shaojun Zhu [a], Mei Yan [a,*], Shenguang Ge [b], Jinghua Yu [a]

[a] School of Chemistry and Chemical Engineering, University of Jinan, Jinan 250022, PR China
[b] Shandong Provincial Laboratory of Preparation and Measurement of Building Materials, University of Jinan, Jinan 250022, PR China

ARTICLE INFO

Article history:
Received 22 June 2016
Received in revised form
28 July 2016
Accepted 5 August 2016
Available online 5 August 2016

Keywords:
3D origami electrochemical device
$(Fe\text{-}P)_n$-MOF-Au-GR
Pb^{2+} detection

ABSTRACT

A highly sensitive electrochemical (EC) biosensor combined with a 3D origami device for detection of Pb^{2+} was developed based on novel Au nanoparticles modified paper working electrode (Au-PWE) as sensor platform and DNA functionalized iron-porphyrinic metal-organic framework ((Fe-P)n-MOF-Au-GR) hybrids as signal probes. In the presence of Pb^{2+}, GR could be specifically cleaved at the ribonucleotide (rA) site, which produced the short $(Fe\text{-}P)_n$-MOF-linked oligonucleotide fragment to hybridize with hairpin DNA immobilized on the surface of Au-PWE. Because of the mimic peroxidase property of $(Fe\text{-}P)_n$-MOF, enzymatically amplified electrochemical signal was obtained to offer the sensitive detection of Pb^{2+}. In addition, benefiting from the Pb^{2+} dependent GR, the proposed assay could selectively detect Pb^{2+} in the presence of other metal ions. This method showed a good linear relationship between the current response and the Pb^{2+} concentration ranging from 0.03 to 1000 nmol L^{-1} with a detection limit of 0.02 nmol L^{-1}. The Au-PWE based electrochemical sensor along with the $(Fe\text{-}P)_n$-MOF-Au-GR probe exhibited the advantages of low-cost, simple fabrication, high sensitivity and selectivity, providing potential application of real-time Pb^{2+} detection both in environmental and biological samples.

1. Introduction

Paper is a biocompatible porous cellulose fiber web with large surface area, and the porous nature fulfills the primary tasks such as diagnostic tests using body fluids and fluid transport. Since microfluidic paper-based analytical devices (μ-PADs) were first reported by White sides' group (Martinez et al., 2010) which offered excellent properties (Abe et al., 2008), including low sample and reagent consumption, low cost, small size, portable and easy-to-operate (Martinez et al., 2007), μ-PADs were considered as ideal platforms designed for point-of-care (POC) detection (Manz et al., 1990; Martinez et al., 2008), To make real POC device, not only the production of low-cost and portable devices were required but also the instrument to measure the signal should be portable (Delaney et al., 2011), Efforts have been made to improve the immobilization of bio-recognition substance in paper (Wu et al., 2013) as well as the signal amplification for paper-based assays (Li et al., 2008). Gold nanoparticles (AuNPs) have attracted much attention in different bio-affinity assays due to their unique physical and chemical properties, such as easily controllable size distribution, long-term stability, superior conductivity, large surface area, and biocompatibility (Dai et al., 2010). Taking into consideration the above advantages, a novel porous Au-paper working electrode (Au-PWE) was developed on a compatibly designed microfluidic origami electrochemical (EC) device through the growth of an interconnected AuNPs layer on the surfaces of cellulose fibers in the paper sample zone to enhance the conductivity of the paper sample zone (Wang et al., 2014a, 2014b).

As an emerging class of highly ordered porous materials, metal-organic frameworks (MOFs) have attracted great attention in the last two decades (Li et al., 1999; Mattos et al., 2012). They have great potential applications in many fields, especially in gas storage/separation, sensing, and catalysis. Recently, prominent progress has been made in the application of luminescent MOF for sensing important targets such as cations, anions, small molecules, gas, and vapors (Corma et al., 2010) (Furukawa et al., 2013; Suh et al., 2012). Linker modification is one of the most direct methods for MOF functionalization (Liu et al., 2012; Jiang et al., 2010; Zou et al., 2012; Jin et al., 2014). Porphyrinic ligands are such a category of versatile linkers that have been extensively explored. These porphyrin derivatives play key roles in many chemical and biological processes (Li et al., 2012). For example, MOF created with porphyrin or porphyrin derivatives have been used to catalyze organic reactions (Lu et al., 2014), including olefin epoxidation (Gao et al., 2014) and CO_2/propylene oxide coupling reactions (Ling et al., 2015a, 2015b). Fe(III)-based MOF have been reported to

* Corresponding author.
E-mail address: chm_yanm@126.com (M. Yan).

http://dx.doi.org/10.1016/j.bios.2016.08.016
0956-5663/

exhibit peroxidase-like catalytic activity and used to construct colorimetric biosensing methods for detection of H_2O_2 and ascorbic acid (Feng et al., 2013). Recently, a porous iron-porphyrinic MOF has been synthesized to show peroxidase activity similar to horse radish peroxidase in an organic solvent (Liu et al., 2013). When MOFs work as platforms to immobilize porphyrin groups, their rigid structures with high surface area and porosity can not only make each porphyrin accessible by substrates but also prevent the dimerization of reaction centers, which will block the catalysis pathway (Mckinlay et al., 2010). Because of the versatility of porphyrin and its promising combination with MOFs, extensive synthetic studies have been reported (Kreno et al., 2012).

Recent study also proves that MOFs could be as a promising candidate for the catalyst of the hydrogen evolution reaction (Hu et al., 2014). In particular, MOF possess intrinsic catalytic activity, and were found to catalyze the reduction reaction procedure of hydrogen peroxide (H_2O_2) (Sugikawa et al., 2013). Gold nanoparticles (AuNPs) are the most useful metal nanoparticles in electrochemical biosensors due to their good biocompatibility and easy functionalization with –SH and $–NH_2$, and large specific surface area, good stability and optical properties (Sugikawa et al., 2011). More importantly, AuNPs provided a good pathway of electron transfer and enhanced the immobilized amount of biomolecules. Hereon, the AuNPs can immobilize on the surface of MOF through animation of silicon dioxide, which can linked with much sensor probs. As a consequence, gold nanoparticles functionalized MOF (MOF-Au) was applied in our work.

As a well-known and nondegradable environmental pollutant, lead cation (Pb^{2+}) can accumulate in human body through the food chain and lead to adverse effects on the immune, central nervous, and reproductive systems, particularly in children (He et al., 2006; Lu et al., 2013). Therefore, different Pb^{2+} sensors have been proposed for sensitive detection of Pb^{2+} by using cost-effective Pb^{2+}-dependent DNAzyme (Wang et al., 2013; Wang and Irudayaraj, 2011) This enzyme is quite stable and can remain its activity or binding ability after repeated denaturation and renaturation (Wei et al., 2008). The detection sensitivity of electrochemical sensors (Cao et al., 2013) for Pb^{2+} can be improved by replacing small redox molecules with signal amplification strategies by employing inorganic nanoparticles combined with additional amplification processes, such as surface preconcentration (Lin et al., 2011) or enzymatic recycling (Tang et al., 2013; Zhang et al., 2015). However, these amplification ways usually need long detection time, and the native enzymes suffer from the certain disadvantages of time-consuming separation and purification, high cost, easy denaturation, and being susceptible to environmental conditions (Chad et al., 2003). Thus, a new detection strategy to produce more signal products with cost efficient and stable enzyme mimic has been considered as another opportunity for electrochemical detection of Pb^{2+} (Gilad et al., 2012; Xiang et al., 2009; Cui et al., 2015).

In the present work, a highly sensitive and selective electrochemical sensor for Pb^{2+} was proposed with a newly designed DNA functionalized iron-porphyrinic MOF. The stable $(Fe\text{-}P)_n$-MOF could produce multisignal species to achieve the high sensitivity, while the GR which was linked to $(Fe\text{-}P)_n$-MOF via the Au nanoparticles (AuNPs), achieved the high selectivity of this method. The good performance showed its potential application for the detection of Pb^{2+} in different environments.

2. Experimental methods

2.1. Preparation of the 3D origami EC device and Au-PWE

The preparation of the 3D origami EC device was similar to our previous work (Martinez et al., 2008) and a detailed procedure was described in Supporting Information. As shown in Scheme 1A, the Au-PWE was fabricated through growth of an Au NPs layer on the surfaces of cellulose fibers in the paper sample zone of PWE to enhance the conductivity and enlarge the effective surface area of bare PWE. The fabrication procedures of the porous Au-PWE were described as follows: First, The suspension of AuNP seeds was prepared by using $NH_4OH \cdot HCl$ as reductant and stabilized with sodium citrate according to the literature. (Busbee et al., 2003) Then, 15.0 μL as-prepared AuNP seeds solution were dropped into the paper sample zone of bare PWE (Scheme 1A), respectively. Then the origami device was equilibrated at room temperature for 1 h to optimize the surface immobilization of AuNP seeds on cellulose fibers. After rinsing with water thoroughly to remove loosely bound AuNP seeds, 15 μL freshly prepared growth aqueous solution of 0.01 mol L^{-1} PBS (pH 7.0) containing 1.2 mmol L^{-1} $HAuCl_4$, 2.0 mmol L^{-1} cetyltrimethylammonium chloride and 7.2 mmol L^{-1} H_2O_2 for seeds growth were applied into the AuNP seeded PWE, and incubated at room temperature for 10 min. Subsequently, the resulting porous Au-PWE was washed with water thoroughly. Thus a layer of interconnected AuNPs on cellulose fibers with good conductivity were obtained (Scheme 1A), which were dried at room temperature for 20 min

2.2. Preparation of (Fe-P)n-MOF and $(Fe\text{-}P)_n$-MOF-Au-GR

The $(Fe\text{-}P)_n$-MOF and $(Fe\text{-}P)_n$-MOF-Au-GR were prepared according to the literature with slight modification: (Jahan et al., 2012; Cui et al., 2015) TMPP (30.22 mg), $FeCl_3 \cdot 6H_2O$ (35.45 mg) and HCl (0.8 mL, 0.1 mol L^{-1} in ethanol) were homogeneously dissolved in a mixture of 3 mL of DMF and 6 mL of ethanol with assistance of sonication treatment. The final mixture was placed into a 40 mL Teflon stainless vessel and was then thermally treated at 150 °C in an oven for 36 h, followed by slow cooling to room temperature. The crystals were collected via filtration and washed with DMF and ethanol, then dried at 60 °C in a vacuum oven.

First, $(Fe\text{-}P)_n$-MOF (4.0 mg) was dispersed in 1 mL of ethanol. This dispersion was added to a mixture of 0.20 mL of ammonium hydroxide (1.00 mol L^{-1}) and 11.3 mL ethanol, and then TEOS (1.5 mL, 6.0 mmol L^{-1}) was added. After the mixture was stirred for reaction at room temperature for 2 h, the products were harvested by centrifuging and washing three times with ethanol and dried under vacuum overnight to get the SiO_2 coated $(Fe\text{-}P)_n$-MOF composite. Then, 4 mg of SiO_2 coated $(Fe\text{-}P)_n$-MOF was added into 4 mL of 20 mmol L^{-1} MPTS ethanol solution and refluxed at 65 °C for 3 h. After centrifugation and washing several times with ultrapure water, the $(Fe\text{-}P)_n$-MOF modified with MPTS was dried at 50 °C for 12 h. The MPTS modified $(Fe\text{-}P)_n$-MOF was further modified with AuNPs by mixing 4 mL of AuNPs (13 nm diameter) solution with 2 mL of MPTS modified $(Fe\text{-}P)_n$-MOF (1 mg mL^{-1}) and shaking vigorously for 2 h. The formed $(Fe\text{-}P)_n$-MOF-Au composite was collected by centrifugation, washed with ultrapure water three times, and dispersed in 6 mL of 50 mmol L^{-1} Tris-acetate buffer (pH 7.0).

A volume of 100 μL of GR (10 μmol L^{-1}, in 50 mmol L^{-1} pH 8.2 Trisacetate buffer containing 300 mmol L^{-1} NaCl) was heated at 95 °C for 10 min and then cooled to room temperature. After the treated GR was activated with 5 μL of 10 mmol L^{-1} TCEP to reduce disulfide bond, it was mixed with 500 μL of $(Fe\text{-}P)_n$-MOF-Au suspension to incubated for 24 h at room temperature to obtain $(Fe\text{-}P)_n$-MOF-Au-GR probe, which was blocked with 1% BSA for 1 h and dispersed in 500 μL of 50 mmol L^{-1} Tris-acetate buffer (containing 300 mmol L^{-1} NaCl, pH 7.0) to store at 4 °C before use (as shown in Scheme 1B).

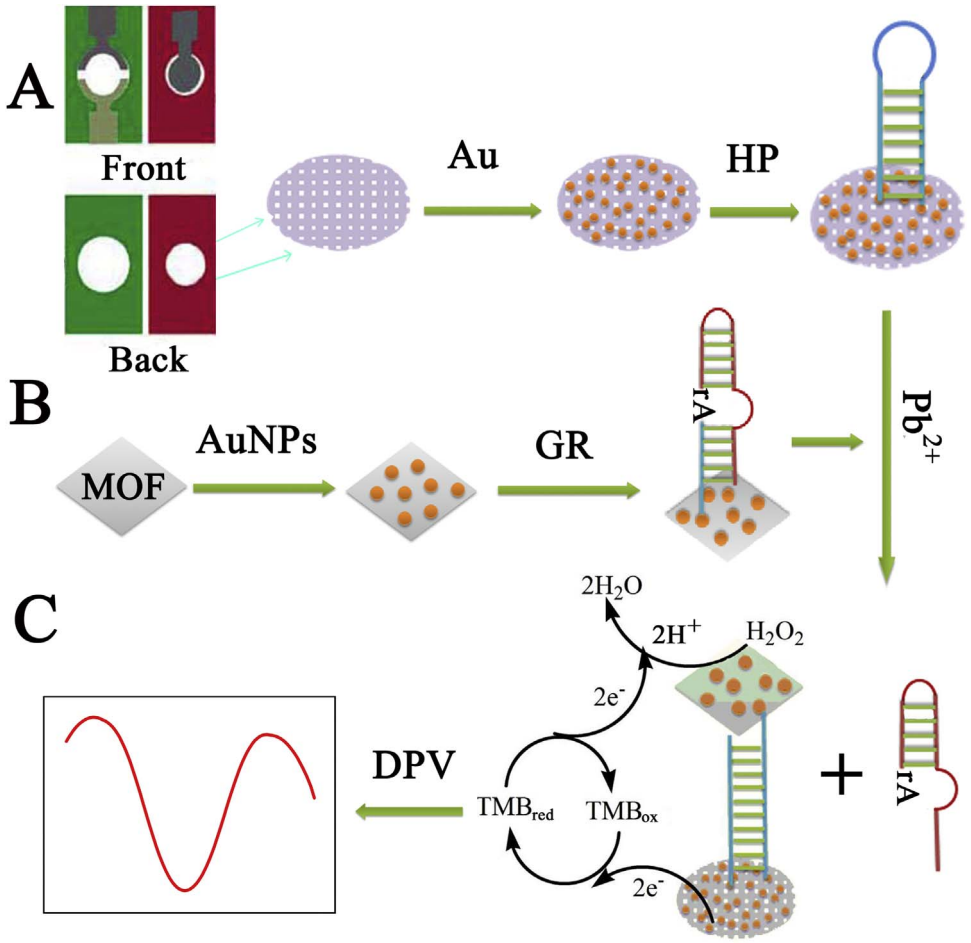

Scheme 1. Fabrication process of the electrochemical biosensor.

2.3. Detection of Pb^{2+}

A volume of 10 μL of HP was dropped onto the Au-PWE and incubated at 37 °C for 90 min. After, 10 μL of Pb^{2+} at various concentrations or samples and 90 μL of $(Fe\text{-}P)_n$-MOF-Au-GR probe were mixed in 50 mmol L^{-1} Tris-acetate buffer (300 mmol L^{-1} NaCl, pH 7.0). Then, 10 μL of the mixture was dropped onto the HP modified electrode and incubated at 37 °C for 90 min. After washing with 50 mmol L^{-1} Tris-acetate buffer (pH 7.0), 50 μL of 0.1 mol L^{-1} pH 5.5 HAc-NaAc buffer containing 0.90 mmol L^{-1} TMB and 0.50 mmol L^{-1} H_2O_2 was added on the sensor surface. They were showed in Scheme 1C, measurements were immediately made with a DPV method.

3. Results and discussion

3.1. Characterization of the Au-PWE

The modification process of the resulting PWE could be observed on the SEM and TEM images. As shown in Fig. 1, the porous bare paper sample zone (Fig. 1A), possessing a high ratio of surface area to weight (9.5 m^2 g^{-1}) (Pelton, 2009) with rough cellulose fibers, could offer an excellent adsorption microenvironment for the AuNP seeds (Fig. 1B). After 40 min of growth, a continuous and dense Au conducting layer was observed on the cellulose fiber surfaces in the paper sample zone (Fig. 1D–F). The TEM image of the as-prepared AuNP seeds is shown in Fig. 1C, the average diameter was ~13 nm.

3.2. Characterization of $(Fe\text{-}P)_n$-MOF and $(Fe\text{-}P)_n$-MOF-Au

The $(Fe\text{-}P)_n$-MOF consisted of a rod shape-like crystal with the width of 100–200 nm (Fig. 2A). As shown in Fig. 2B and C, the AuNPs with an average diameter of 13 nm (Fig. 1C) were well dispersed on the surface of $(Fe\text{-}P)_n$-MOF matrix, conforming the successful modification of AuNPs on $(Fe\text{-}P)_n$-MOF. From the HRTEM of $(Fe\text{-}P)_n$-MOF (Fig. 2D), the more detail structures can be seen clearly. XRD method was used to examine the phase and structure of the $(Fe\text{-}P)_n$-MOF and $(Fe\text{-}P)_n$-MOF-Au. As shown in Fig. 2E (a), the diffraction peaks around 9.46°, 18.49°, 23.96° and 31.21° were observed, which corresponded to the (100), (200), (111), and (121) planes, and in Fig. 2E (b), the curve exhibited another two diffraction peaks at 38.33° and 44.18°, which can be indexed to diffraction from the (111) and (220) of the fcc structure of metallic Au, respectively (Jahan et al., 2012; Wang et al., 2014a, 2014b). This result was coincident with that of the previously reported MOF and Au, indicating the synthesized $(Fe\text{-}P)_n$-MOF exhibited well-recognized crystalline diffraction patterns. The morphologies of $(Fe\text{-}P)_n$-MOF played a critical role in the preparation of mimic enzyme (Ling et al., 2015a, 2015b). To further monitor the formation of $(Fe\text{-}P)_n$-MOF-Au, the FT-IR spectra (Fig. S2) and UV–vis absorption spectrum (details in Supporting information) of the AuNPs-$(Fe\text{-}P)_n$-MOF was also investigated (Fig. 2F).

3.3. Peroxidase-like catalytic performance of $(Fe\text{-}P)_n$-MOF

The electrochemical properties of the resulted porous Au-PWE

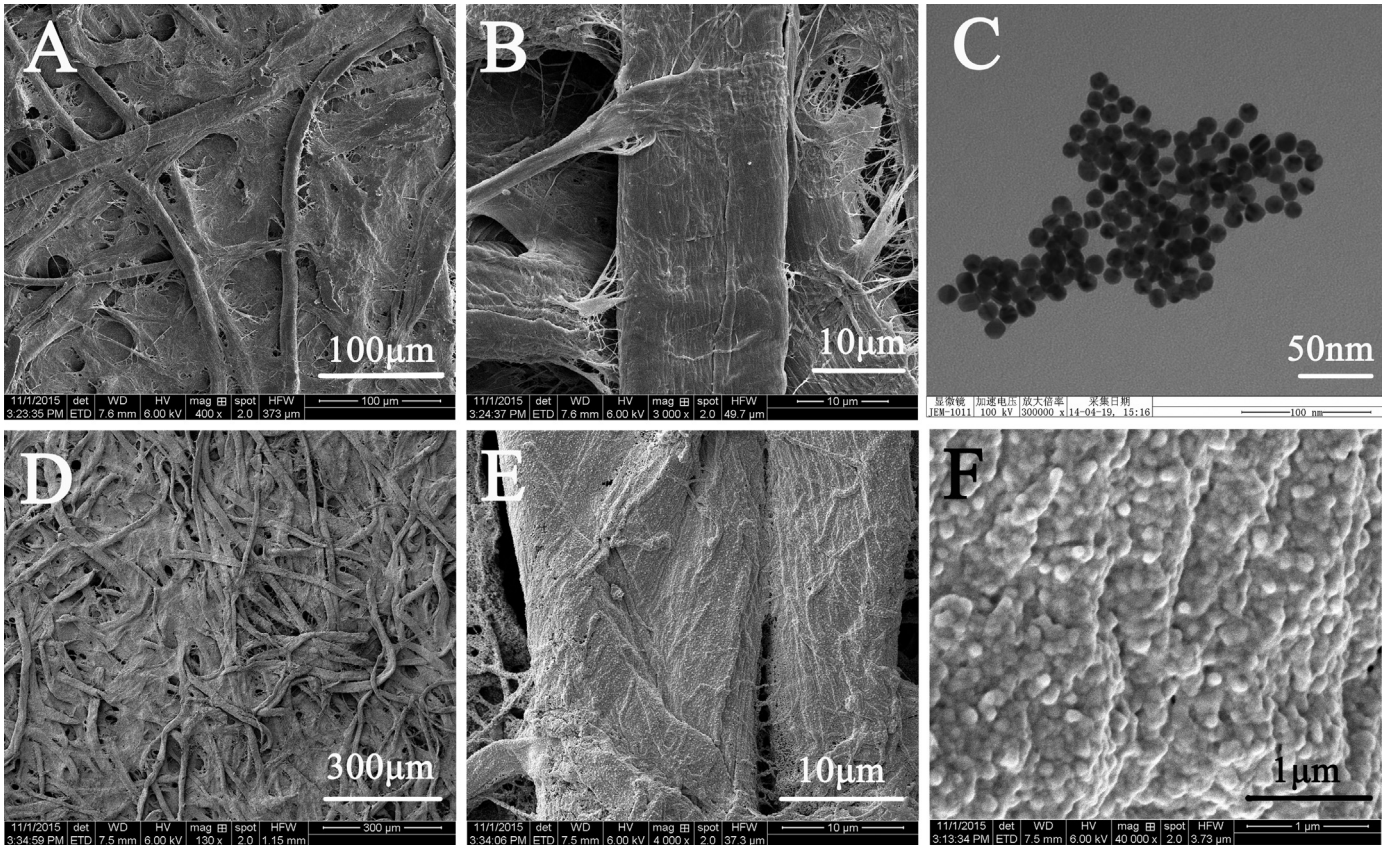

Fig. 1. (A and B) SEM images of the pure cellulose paper under different magnification, (C) TEM image of AuNPs, (D, E and F) SEM images of Au-PWE under different magnification.

were investigated in Supporting Information. The peroxidase-like catalytic performance of $(Fe\text{-}P)_n$-MOF was evaluated with an typical colorimetric oxidation reaction of TMB by H_2O_2 (Fig. S4A). The $(Fe\text{-}P)_n$-MOF could be well dispersed in water to form a homogeneous suspension with black color. Upon the addition of 5 μL of 1 mg mL^{-1} $(Fe\text{-}P)_n$-MOF suspension to 500 μL of the mixture of TMB and H_2O_2, TMB molecule lost one electron and transformed into the status of cation radical, then the colorless solution turned to blue color immediately, indicating $(Fe\text{-}P)_n$-MOF possessed the peroxidase-like activity to catalyze the oxidation of TMB in the presence of H_2O_2 (Wu et al., 2011). Like the oxidation reaction catalyzed by peroxidase, the catalytic activity of $(Fe\text{-}P)_n$-MOF could be stopped by H_2SO_4, leading to the cation radical of TMB molecule, which further lost another electron to form diamine, and the blue solution changed to be yellow. These changes The catalytic performance of $(Fe\text{-}P)_n$-MOF for oxidation of TMB by H_2O_2 was further confirmed by electrochemical measurements (Fig. S4B). Compared with the CV response of TMB on bare Au-PWE (curve a), the CV response on $(Fe\text{-}P)_n$-MOF modified Au-PWE showed the increase of the reduction peak current (curve b), indicating a typical electrocatalytic process, which was attributed to the enzymatic catalysis of the immobilized $(Fe\text{-}P)_n$-MOF to the oxidation reaction of TMB by H_2O_2. The mechanism of enzymatic catalysis was similar to that with natural or the mimetic peroxidase reported previously. Accordingly, a significant reduction current was obtained on $(Fe\text{-}P)_n$-MOF modified Au-PWE by DPV detection at 0.2–0.8 V (Fig. S4C), the Au-PWE expressed a very weak current (curve a), but the $(Fe\text{-}P)_n$-MOF modified electrode revealed excellent current performance (curve b). The results indicated that the $(Fe\text{-}P)_n$-MOF composite had larger surface area and fascinating electrocatalytic activity, which facilitated the DPV measure. Therefore, the $(Fe\text{-}P)_n$-MOF modified electrode had highly effective electrochemistry properties, which were promising for the construction of biosensor.

3.4. Stability of $(Fe\text{-}P)_n$-MOF

A favorable mimic enzyme should process good catalytic ability in broad conditions. After the natural enzyme (HRP), and $(Fe\text{-}P)_n$-MOF modified Au-PWE were exposed to different pH ranging from 3 to 10 (Fig. 3A) and temperature ranging from 4 to 60 °C (Fig. 3B) for 2 h, their relative activities were measured in the detection solution. After exposure to pH 3.0 and 10.0 solution for 2 h, the catalytic activity of $(Fe\text{-}P)_n$-MOF could remain of 46.9% and 40.5%, respectively (curve a), while the HRP remained only 8.2% of their activity at pH 3.0, 5.0% of its activity at pH 10.0, respectively (curves b). The effect of the temperature on its stability showed similar phenomena. In the temperature range of 4–60 °C, the $(Fe\text{-}P)_n$-MOF was stable and remained at 80.7% of its activity at 60 °C (curve a), but HRP showed narrow temperature ranges for their remaining activity and remained at 36.7% of its activity at 60 °C, respectively (curves b). Obviously, $(Fe\text{-}P)_n$-MOF was more favorable in a wider range of pH and temperature than HRP that was very sensitive to pH and temperature, suggesting that $(Fe\text{-}P)_n$-MOF had a great potential application in bioanalysis.

3.5. Electrochemical behavior of the biosensor

EIS was an effective method for probing the features of surface modified electrodes. The impedance spectra included a semicircle portion and a linear portion. The semicircle diameter at higher frequencies corresponds to the electron-transfer resistance (R_{et}), and the linear part at lower frequencies corresponds to the diffusion process, the details were in Supporting Information. As

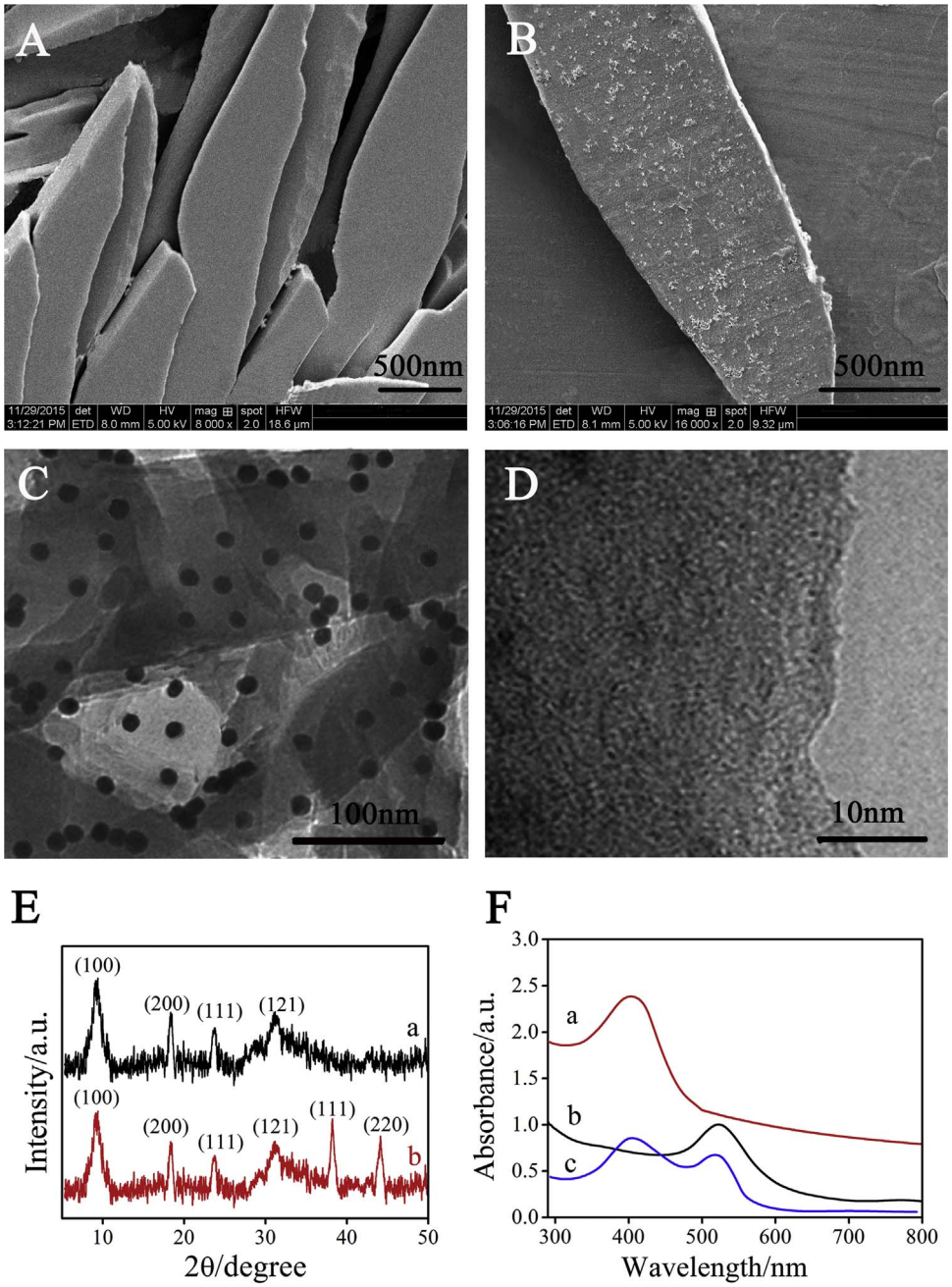

Fig. 2. (A) SEM image of $(Fe\text{-}P)_n$-MOF, (B) SEM image of $(Fe\text{-}P)_n$-MOF-Au, (C) TEM of $(Fe\text{-}P)_n$-MOF-Au, (D) HRTEM of $(Fe\text{-}P)_n$-MOF, (E) XRD of $(Fe\text{-}P)_n$-MOF (a) and $(Fe\text{-}P)_n$-MOF-Au (b), (F) UV–vis absorption spectra of (a) $(Fe\text{-}P)_n$-MOF, (b) AuNFs, and (c) $(Fe\text{-}P)_n$-MOF-Au composite.

shown in Fig. 3C the results were consistent with the fact that this 3D origami EC device was fabricated as expected.

3.6. Sensitivity of the electrochemical biosensor

A volume of 10 μL of Pb^{2+} at various concentrations and 90 μL of $(Fe\text{-}P)_n$-MOF-Au-GR probe were mixed in 50 mmol L^{-1} Tris-acetate buffer (300 mmol L^{-1} NaCl, pH 7.0). Then, 10 μL of the mixture was dropped onto the HP modified electrode and incubated at 37 °C for 90 min. After washing with 50 mmol L^{-1} Tris-acetate buffer (pH 7.0), 50 μL of 0.1 mol L^{-1} pH 5.5 HAc-NaAc buffer containing 0.90 mmol L^{-1} TMB and 0.50 mmol L^{-1} H_2O_2 was added on the sensor surface. In the presence of Pb^{2+}, GR could be specifically cleaved at the ribonucleotide (rA) site, which produced the short $(Fe\text{-}P)_n$-MOF-linked oligonucleotide fragment to hybridize with hairpin DNA immobilized on the surface of Au-PWE. Because of the mimic peroxidase property of $(Fe\text{-}P)_n$-MOF, enzymatically amplified electrochemical signal was obtained to offer the sensitive detection of Pb^{2+}. Fig. 4A the current intensity of the solution in the absence (a) and presence (b∼k) of different concentrations of Pb^{2+}. It can be seen that the current intensity in the presence of Pb^{2+} (b) was higher than that in the absence of Pb^{2+} (a), and the current intensity increased gradually with increasing concentrations of Pb^{2+} (b∼k). The reason was that the specific binding of HP and GR with the Pb^{2+}, and thus added TMB and H_2O_2 increased the current intensity, which suggested that the Pb^{2+} concentration could be determined by the DPV measurement of this reaction. The standard calibration curve for the Pb^{2+} detection is shown in Fig. 4B and C. The current intensity increased linearly with the logarithm value of Pb^{2+} concentration from 0.03

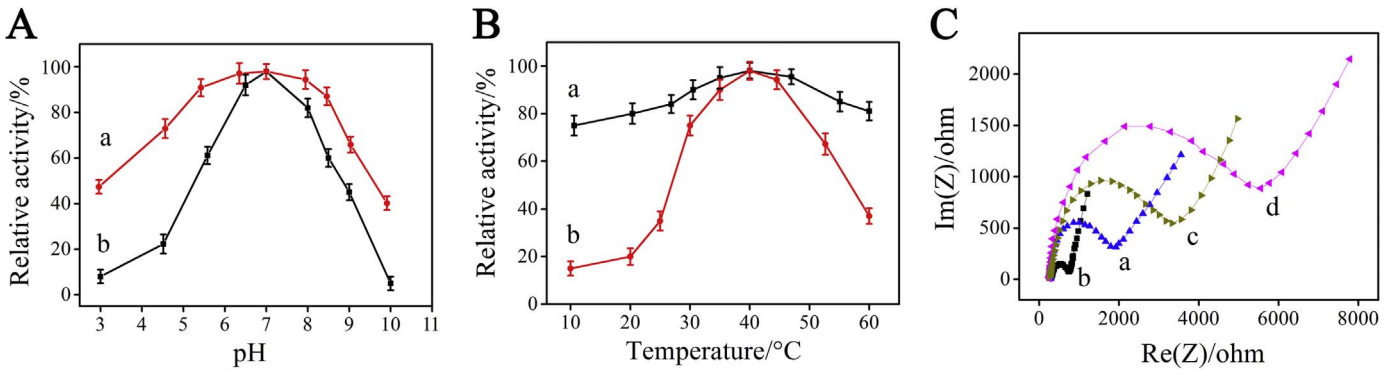

Fig. 3. Relative electrocatalytic activity of (a) $(Fe\text{-}P)_n$-MOF and (b) HRP modified Au-PWE in 0.1 mol L^{-1} HAc-NaAc buffer containing 0.90 mmol L^{-1} TMB and 0.50 mmol L^{-1} H_2O_2 after exposure to different (A) pH at 37 °C and (B) temperature at pH 7.0 for 2 h, (C) EIS of bare PWE (a), Au-PWE (b), Au-PWE-HP (c), and $(Fe\text{-}P)_n$-MOF-Au-GR (d) with 0.01 mol L^{-1} PBS (2.5 mmol L^{-1} $Fe(CN)_6^{4-/3-}$ +0.1 mol L^{-1} KCl). The frequency range is between 0.01 and 100,000 Hz with signal amplitude of 5 mV.

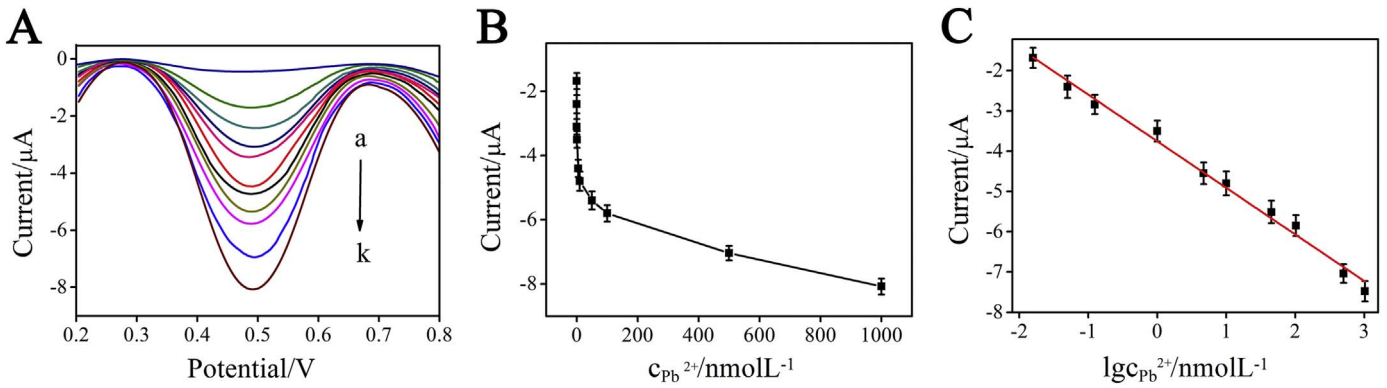

Fig. 4. (A) DPV profiles of the biosensor in the absence (a-k) of different concentrations of Pb^{2+} in pH 7.0 PBS, (B) the quantity of the biosensor, (C) the calibration curve of the biosensor, Pb^{2+} concentration (nmol L^{-1}): (a) 0, (b) 0.03, (c) 0.5, (d) 0.1, (e) 1, (f) 5, (g) 10, (h) 50, (i) 100, (j) 500, (k) 1000.

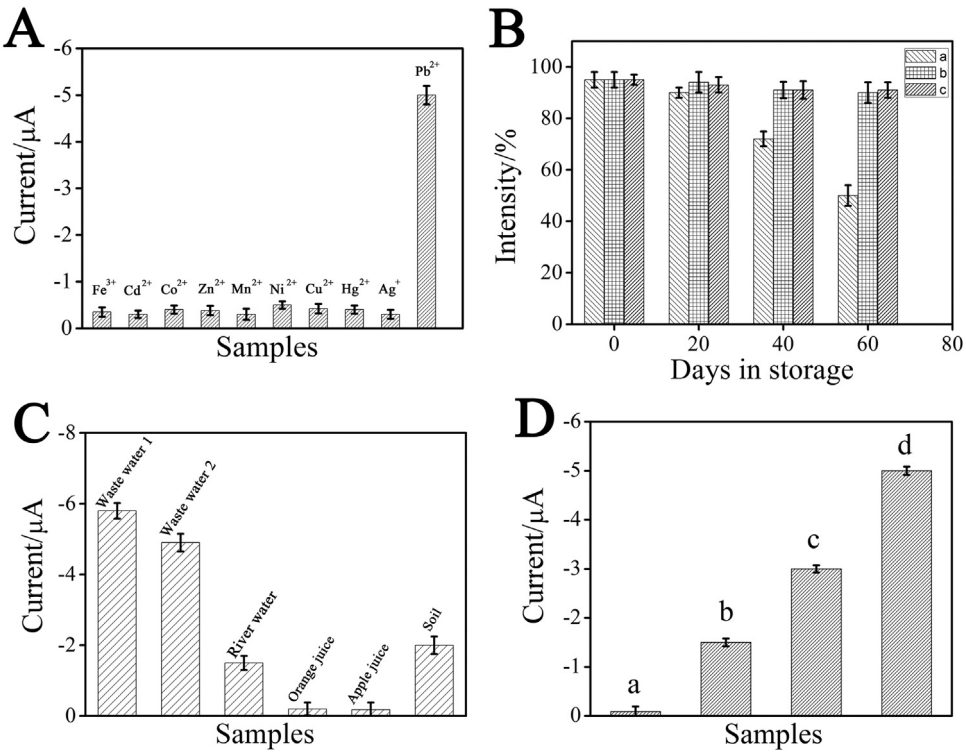

Fig. 5. (A) Selectivity of the biosensor, (B) the storage stability of the biosensor (a) at room temperature, (b) in a refrigerator and (c) in a freezer, (C) real samples detection, (D) human serum samples with different concentrations of Pb^{2+}: (a) 0 nmol L^{-1} (b) 0.05 nmol L^{-1}, (c) 0.1 nmol L^{-1}, (d) 20 nmol L^{-1}.

to 1000 nmol L^{-1} with a detection limit of 0.02 nmol L^{-1}. The linear fit equation is Current = −3.75 − 1.16 $lgc_{Pb}{}^{2+}$ (unit of c is nmol L^{-1}), with a correlation coefficient of 0.9912. According to the linear equation, we could detect trace Pb^{2+} concentration quantitatively. Which was at least 550 times lower than that of 10 μg L^{-1} in drinking water permitted by World Health Organization (Martinis et al., 2010). The detection limits of the proposed and previously reported sensors were compared in Table S1. The detection limit of the proposed sensor was much lower than those of other electrochemical methods and much superior to the fluorescent and colorimetric sensors for Pb^{2+}. This result indicated that the artificial enzyme was able to replace the redox label to amplify the signal through the catalytic reaction.

3.7. Selectivity and stability of the electrochemical sensor

To investigate the selectivity, the sensor was determined by exposing it to several metal ions including Fe^{3+}, Cd^{2+}, Co^{2+}, Zn^{2+}, Mn^{2+}, Ni^{2+}, Cu^{2+}, Hg^{2+} and Ag^{+} (Fig. 5A). In order to study the interfering effects or selectivity of the procedure, many of the coexisting species in real waters should be investigated (Fig. S5). A negligible response was observed when the sensor was challenged with above possible interference ions even at a 50-fold higher concentration than Pb^{2+} (5 μmol L^{-1} vs 0.1 μmol L^{-1}). In addition, the current responses of 0.1 μmol L^{-1} Pb^{2+} in the presence of these interfering ions were similar to those without interfering ion. Therefore, the proposed sensor has demonstrated an excellent selectivity for the detection of Pb^{2+}, indicating its potential application for analysis of complex samples.

The storage stability of the biosensors was evaluated by measuring the colorimetric response of the modified papers and the Au-PWE/HP/$(Fe\text{-}P)_n$-MOF-Au-GR stored at room temperature (25 °C), in a refrigerator (4 °C) and in a freezer (−20 °C). Fig. 5B shows the average storage stability under three conditions over a period of days. Then 50 μL of 0.1 mol L^{-1} pH 5.5 HAc-NaAc buffer containing 0.90 mmol L^{-1} TMB and 0.50 mmol L^{-1} H_2O_2 was added on the sensor surface used for each test and each experiment was performed in triplicate. The stability of the biosensors stored at room temperature was 95% of the initial response in the first 20 days and then decreased to 50% in the next 40 days. A remarkable average stability of up to 95% and 94% of the initial response was retained after 60 days of storage in the refrigerator and freezer. The results demonstrate the excellent storage stability of the biosensor.

3.8. Analytical application for determination of Pb^{2+} in real samples

Procedure for the detection of Pb^{2+}. The method in this work was applied for real samples (preparation of real samples in Supporting Information) such as water samples (two industrial waste water samples and one river water sample), fruit juice samples (orange juice and apple juice) and solid samples, as shown in Fig. 5C. And the results were shown in Table S2. Therefore, this method could be reasonably applied in the environmental detection of Pb^{2+}.

3.9. Analytical application for determination of Pb^{2+} in human serum samples

In an attempt to test the applicability of our electrochemical sensor for detection in biological sample matrix, we employed diluted human serum samples (1:10). A volume of 10 μL of serum samples and 90 μL of $(Fe\text{-}P)_n$-MOF-Au-GR probe were mixed in 50 mmol L^{-1} Tris-acetate buffer (300 mmol L^{-1} NaCl, pH 7.0). Then, 10 μL of the mixture was dropped onto the HP modified electrode and incubated at 37 °C for 90 min. After washing with 50 mmol L^{-1} Tris-acetate buffer (pH 7.0), 50 μL of 0.1 mol L^{-1} pH 5.5 HAc-NaAc buffer containing 0.90 mmol L^{-1} TMB and 0.50 mmol L^{-1} H_2O_2 was added on the sensor surface. Then different concentrations of Pb^{2+} solutions were added to the system. Then the current peak of the solution was detected, founding there was little Pb^{2+} in human serum samples. The different of current intensities of the solution was recorded with adding different concentrations of Pb^{2+} (as shown in Fig. 5D). Therefore, this method could be reasonably applied in the biological sample matrixes detection of Pb^{2+}.

4. Conclusions

In summary, we reported a sensitive EC bioanalytical protocol for detection of Pb^{2+} based on Au-PWE as a platform and $(Fe\text{-}P)_n$-MOF-Au-GR hybrids as signal probes. The Au-PWE had a large active surface area and excellent conductivity, which played an essential role in not only binding the hairpin DNA, but also assisting the electron transfer process. This method has a potential in applied for Pb^{2+} determination in various water samples, fruit juice samples and soil sample available in the local, and thus provide a new promising platform for clinical analysis. The resulting μ-PAD EC biosensor, with simple, low cost, ultrahigh sensitivity and satisfactory stability, could be suitable for detection of Pb^{2+}. Furthermore, it will be a suitable probe for efficient monitoring of intracellular Pb^{2+} levels within living organisms. Hence, the proposed microfluidic origami electrochemical biosensor could become a promising method for local market.

Acknowledgement

This work was financially supported by National Natural Science Foundation of China (51273084 and 51473067), Shandong Provincial Excellent Youth Foundation (ZR2015JL019).

Appendix A. Supporting information

Supplementary data associated with this article can be found in the online version at http://dx.doi.org/10.1016/j.bios.2016.08.016.

References

Abe, K., Suzuki, K., Citterio, D., 2008. Anal. Chem. 80, 6928–6934.
Busbee, B.D., Obare, S.O., Murphy, C.J., 2003. Adv. Mater. 15, 414–416.
Cao, S., Zhang, L., Chai, Y., Yuan, R., 2013. Biosens. Bioelectron. 42, 532–538.
Chad, E., Reese, S.A., Asher, P., 2003. Anal. Chem. 75, 3915–3918.
Corma, A., Garciía, H., Llabreés, I., Xamena, F.X., 2010. Chem. Rev. 110, 4606–4655.
Cui, L., Wu, J., Li, J., Ju, H.X., 2015. Anal. Chem. 87, 10635–10641.
Dai, X.J., Luo, Y.S., Zhang, W.D., Fu, S.Y., 2010. Dalton Trans. 39, 3426–3432.
Delaney, J.L., Hogan, C.F., Tian, J.F., Shen, W., 2011. Anal. Chem. 83, 1300–1306.
Feng, D., Chung, W.C., Wei, Z., Gu, Z.Y., Jiang, H.L., Chen, Y.P., Darensbourg, D.J., Zhou, H.C., 2013. J. Am. Chem. Soc. 135, 17105–17110.
Furukawa, H., Cordova, K.E., O'Keeffe, M., Yaghi, O.M., 2013. Science 341, 974–975.
Gao, W.Y., Chrzanowski, M., Ma, S.Q., 2014. Chem. Soc. Rev. 43, 5841–5866.
Gilad, P., Ran, T.V., Itamar, W., 2012. Anal. Chem. 84, 3703–3709.
He, Q.W., Miller, E.W., Wong, A.P., Chang, C.J., 2006. J. Am. Chem. Soc. 128, 9316–9317.
Hu, Y.L., Liao, J., Wang, D.M., Li, G.K., 2014. Anal. Chem. 86, 3955–3963.
Jahan, M., Bao, Q., Loh, K.P., 2012. J. Am. Chem. Soc. 134, 6707–6713.
Jiang, H.L., Tatsu, Y., Lu, Z.H., Xu, Q., 2010. J. Am. Chem. Soc. 132, 5586–5587.
Jin, L.N., Liu, Q., Yang, Y., Fu, H.G., Sun, W.Y., 2014. J. Colloid Interface Sci. 426, 1–8.
Kreno, L.E., Leong, K., Farha, O.K., Allendorf, M., Duyne, R.P.V., Hupp, J.T., 2012. Chem. Rev. 112, 1105–1125.
Li, H., Eddaoudi, M., O'Keeffe, M., Yaghi, O.M., 1999. Nature 402, 276–279.
Li, J.R., Sculley, J., Zhou, H.C., 2012. Chem. Rev. 112, 869–932.
Li, Y., Sasaki, T., Shimizu, Y., Koshizaki, N., 2008. J. Am. Chem. Soc. 130, 14755–14762.
Lin, Z.Z., Li, X.H., Kraatz, H.B., 2011. Anal. Chem. 3, 6896–6901.

Ling, P.H., Lei, J.P., Ju, H.X., 2015a. Biosens. Bioelectron. 71, 373–379.
Ling, P.H., Lei, J.P., Zhang, L., Ju, H.X., 2015b. Anal. Chem. 87, 3957–3963.
Liu, J., Thallapally, P.K., McGrail, B.P., Brown, D.R., Liu, J., 2012. Chem. Soc. Rev. 41, 2308–2322.
Liu, Y.L., Zhao, X.J., Yang, X.X., Li, Y.F., 2013. Analyst 138, 4526–4531.
Lu, W.G., Wei, Z.W., Gu, Z.Y., Liu, T.F., Park, J., Park, J., Tian, J., Zhang, M., Zhang, Q., Gentle, T., Bosch, M., Zhou, H.C., 2014. Chem. Soc. Rev. 43, 5561–5593.
Lu, Y., Li, X., Wang, G.K., Tang, W., 2013. Biosens. Bioelectron. 39, 231–235.
Manz, A., Graber, N., Widmer, H.M., 1990. Sens. Actuators B: Chem. 1, 244–248.
Martinez, A.W., Phillips, S.T., Butte, M.J., Whitesides, G.M., 2007. Angew. Chem. Int. Ed. 46, 1318–1320.
Martinez, A.W., Phillips, S.T., Whitesides, G.M., 2010. Anal. Chem. 82, 3–10.
Martinez, A.W., Phillips, S.T., Wiley, B.J., Gupta, M., Whitesides, G.M., 2008. Lab. Chip 8, 2146–2150.
Martinis, E.M., Bertón, P., Altamirano, J.C., Hakala, U., Wuilloud, R.G., 2010. Talanta 80, 2034–2040.
Mattos, L.V., Jacobs, G., Davis, B.H., Noronha, F.B., 2012. Chem. Rev. 112, 4094–4123.
McKinlay, A.C., Morris, R.E., Horcajada, P., Ferey, G., Gref, R., Couvreur, P., Serre, C., 2010. Angew. Chem., Int. Ed. 49, 6260–6266.
Pelton, R., 2009. Anal. Chem. 28, 925–942.
Sugikawa, K., Furukawa, Y., Sada, K., 2011. Chem. Mater. 23, 3132–3134.
Sugikawa, K., Nagata, S., Furukawa, Y., Kokado, K., Sada, K., 2013. Chem. Mater. 25, 2565–2570.
Suh, M.P., Park, H.J., Prasad, T.K., Lim, D.W., 2012. Chem. Rev. 112, 782–835.
Tang, S.R., Tong, P., Li, H., Tang, J., Zhang, L., 2013. Biosens. Bioelectron. 42, 608–611.
Wang, H.B., Wang, L., Huang, K.J., Xu, S.P., Wang, H.Q., Wang, L.L., Liu, Y.M., 2013. New J. Chem. 37, 2557–2563.
Wang, X., Bian, Z.Q., Chu, C.C., Zheng, X.X., Ge, S.G., Yu, J.H., Yan, M., Song, X.R., 2014a. RSC Adv. 4, 52796–52803.
Wang, Y., Irudayaraj, J., 2011. Chem. Commun. 47, 4394–4396.
Wang, Z.F., Liu, N., Ma, Z.F., 2014b. Biosens. Bioelectron. 53, 324–329.
Wei, H., Li, B.L., Li, J., Dong, S.J., Wang, E.K., 2008. Nanotechnology 19, 1–5.
Wu, P., Cai, Z.W., Chen, J., Zhang, H., Cai, Ch.X., 2011. Biosens. Bioelectron. 26, 4012–4017.
Wu, Y.F., Xue, P., Kang, Y.J., Hui, K.M., 2013. Anal. Chem. 85, 3166–3173.
Xiang, Y., Tong, A.J., Lu, Y., 2009. J. Am. Chem. Soc. 131, 15352–15357.
Zhang, P., Wu, X.Y., Yuan, R., Chai, Y.Q., 2015. Anal. Chem. 87, 3202–3207.
Zou, C., Zhang, Z.J., Xu, X., Gong, Q.H., Li, J., Wu, C.D., 2012. J. Am. Chem. Soc. 134, 87–90.